A Switchable Band RF/Analog Processing Single-Sideband Mixer for Distributed Array Phase Synchronization

Hao Yan, *Student Member, IEEE*, Hanxiang Zhang, *Student Member, IEEE*, Powei Liu, *Student Member, IEEE*, and Bayaner Arigong, *Senior Member, IEEE*

***Abstract*— In this article, a sideband switchable RF/analog processing single sideband (SSB) mixer is proposed to synchronize the phase in open-loop distributed array system. The proposed SSB mixer is composed of single balanced mixer, Wilkinson power divider, switches, transmission line delays, RF Hilbert transformer, and T-junction combiner. The design theory is developed for phase synchronization in distributed array based on the sequential switched sideband signal, and detail design approach is developed for the proposed RF/analog processing switchable SSB mixer. By switching the transmission line delays, different sidebands are controlled in the proposed SSB mixer. To verify the design concept, a prototype SSB mixer is designed and validated in simulation and experiment, and the results align well with design theory. Different from other SSB mixer, this is first time a RF/analog processing switchable band SSB mixer is proposed to show great potential for exploring novel wireless communication technique.**

***Index Terms*— Open-loop distributed array, phase synchronization, RF Hilbert transformer, RF signal processing, single sideband (SSB) mixer.**

I. Introduction

IMPROVING wireless connectivity performance as signal-to-noise ratio, throughput, capacity, spectrum efficiency, data rate, coverage, and system power consumption is critical in emerging wireless network, including 5G/NextG, radar, remote sensing, Internet of Things, and vehicle to vehicle. Beamforming is a key technique to focus the radio signal energy in the desired direction, so that it can enhance the signal quality and improve the spectrum efficiency as well reduce the system power consumption. Conventional beamforming is realized on a single platform using phased array antennas [1], [2], [3], [4], [5], [6], where the half-wavelength spaced antenna elements are excited by a locally generated signal with progressive phase difference and desired magnitude response. A distributed transmitter array system [7], [8], [9] is another approach for adding up the energy from physically separated wireless nodes and focusing in a desired direction at long distance. To form this virtual beamforming array, the electrical state of each wireless node is required to be synchronized, especially for frequency and phase of the local oscillator (LO) in each node. Based on the synchronization methodology, two types of distrusted array systems are extensively investigated. First, a closed-loop distributed array is proposed in [10], [11], [12], [13], and [14], where the wireless nodes adjust their electrical state based on the feedback signal from the central base station. Second, an open-loop distributed array is presented in [13], [15], [16], [17], and [18], where the frequency and phase of each node are synchronized by broadcasting a two-tone waveform in neighboring nodes without relying on external feedback signals. In this open-loop distributed array, a self-mixing circuit is applied to demodulate the two-tone waveform for synchronization of secondary nodes. In the RF chain, the mixing circuit or frequency conversion circuit is a key component, and it converts the input signal to two signals and some spurious frequency components. Currently, with the limited spectrum allocation and congested bands, improving spectrum efficiency is becoming a serious issue, especially with the increasing demand for high-speed data streaming and the proliferation of mobile devices. Therefore, to remove the redundant signals generated by the mixer, a spectrum efficient single sideband (SSB) mixer has been developed. The typical topology of SSB mixers [19], [20], [21], [22], [23] includes either two mixers and two 90° hybrid couplers to create in-phase and quadrature signal paths and cancel out one sideband signal or incorporate a filter with sharp cutoff edge to suppress one sideband directly. These SSB mixers feature a complex circuit topology and cancel only one sideband, with no sideband configuration capabilities.

Recently, manipulating the electromagnetic waveform directly in its analog domain attracts great interest to perform various mathematical operations, such as integration [24], differentiation [25], time inversion [26], Fourier transformation [27], edge detection [28], and Hilbert transformation [29], [30], [31]. Inspired by the concept of RF signal processing, in our work presented at the International Microwave Symposium (IMS) 2024, a novel RF/analog processing SSB

Received 15 September 2024; revised 21 October 2024; accepted 24 October 2024. Date of publication 7 November 2024; date of current version 7 January 2025. This work was supported in part by the National Science Foundation (NSF) under Award ECCS-2124531, Award CCF-2124525, and Award ECCS-2340268. This article is an expanded version from the IEEE MTT-S International Microwave Symposium (IMS), Washington, DC, USA, 16–21 June 2024. *(Corresponding author: Bayaner Arigong.)*

The authors are with the Department of Electrical and Computer Engineering, College of Engineering, Florida A&M University-Florida State University, Tallahassee, FL 32310 USA (e-mail: barigong@eng.famu.fsu.edu).

Color versions of one or more figures in this article are available at https://doi.org/10.1109/TMTT.2024.3487917.

Digital Object Identifier 10.1109/TMTT.2024.3487917

mixer topology is proposed by leveraging an RF Hilbert transformer [32]. To further expand the design concept, in this extend paper, a switchable sideband SSB mixer topology is proposed to synchronize the phase of wireless nodes in open-loop distributed array. As shown in Fig. 1, the primary node broadcasts higher sideband (HSB) signal and lower sideband (LSB) signal sequentially via the proposed switchable SSB mixer, and the secondary nodes adjust their electrical status from the received modulated SSB signal, which not only streamlines the transmission process but also significantly reduces spectral overlap and interference, thereby maximizing the efficiency of spectrum utilization. The novelty and contributions of this extended work are summarized as follows.

1) This is the first time an RF/analog signal processing SSB mixer with a switchable sideband is proposed to not only overcome the issues in conventional SSB mixers, where well-matched I/Q mixers and bulky low-frequency intermediated frequency (IF) couplers are required to suppress LO feedthrough and spurious frequencies but also break the limitation of fixed sideband in conventional SSB mixer.
2) By employing this novel SSB mixer, sequentially switched SSB signals are generated to synchronize the phases of the primary node and secondary nodes in large wireless network, thereby realizing an open-loop distributed array system. This article is organized as: Section II provides the design theory of phase synchronization in open-loop distributed array system using sequential switchable SSB signals and the proposed RF/analog processing band switchable SSB mixer; then, Section III discusses the experimental validation of the proposed switchable band RF/analog processing SSB mixer circuit. Finally, Section IV concludes the design theory and experimental results.

II. Design Theory of Switchable Band RF/Analog Signal Processing SSB Mixer and Phase Synchronization in Open-Loop Distribute Array

A. Theory of Phase Synchronization in Distributed Array Applying Sequential Switched SSB Signals

First, a new open-loop distributed array phase synchronization approach is proposed from sequentially switched sideband signals, which addresses the needs of a switchable SSB mixer. As shown in Fig. 1, the primary node in the distributed array generates primary RF signals with carrier frequencies sequentially alternating between the LSB and HSB, which are received simultaneously by both the target and the secondary nodes. Upon receiving the order of HSB and LSB signals, the secondary nodes can extract the phase difference between two sideband signals, where the difference originates from the LO in each node and the varying transmission distances between the primary and secondary nodes. The phase difference between the primary node LO and secondary nodes is denoted as ϕ_c, and the distance between the primary and secondary nodes is noted as dis. The phase difference caused by the distance at the frequencies of the lower side band (f_{LSB})

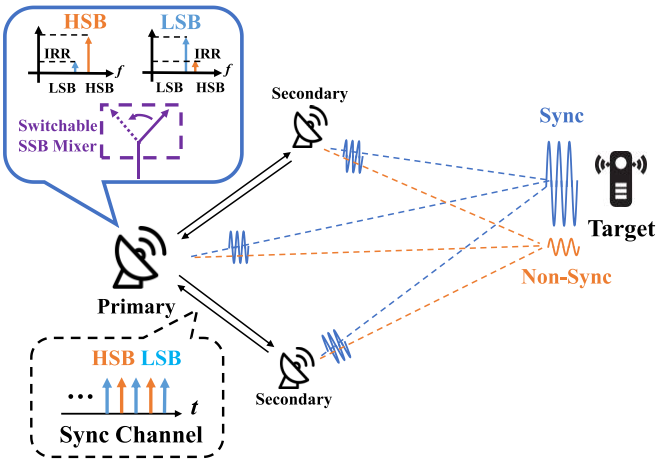

Fig. 1. Phase synchronization in open-loop distributed array applying the proposed switchable sideband SSB mixer.

and higher side band (f_{HSB}) is represented as ϕ_{LSB} and ϕ_{HSB}, which can be derived as

$$\phi_{\mathrm{LSB}} = 2\pi f_{\mathrm{LSB}} \frac{\mathrm{dis}}{c} \tag{1}$$

$$\phi_{\mathrm{HSB}} = 2\pi f_{\mathrm{HSB}} \frac{\mathrm{dis}}{c} \tag{2}$$

where c is the speed of light.

After down conversion, in time domain, the IF signals received in the secondary node are noted as $\mathrm{IF}_{\mathrm{LSB}}$ and $\mathrm{IF}_{\mathrm{HSB}}$, and they can be expressed using ϕ_c, ϕ_{LSB}, ϕ_{HSB}, and ϕ_{LSB} as

$$\mathrm{IF}_{\mathrm{LSB}}(t) = 0.5 \cdot \cos[2\pi(f_{\mathrm{LO}} - f_{\mathrm{LSB}})t + (\phi_c - \phi_{\mathrm{LSB}})] \tag{3}$$

$$\mathrm{IF}_{\mathrm{HSB}}(t) = 0.5 \cdot \cos[2\pi(f_{\mathrm{HSB}} - f_{\mathrm{LO}})t + (\phi_{\mathrm{HSB}} - \phi_c)]. \tag{4}$$

After sampling and Fourier transformation, the value of $(\phi_c - \phi_{\mathrm{LSB}})$ and $(\phi_{\mathrm{HSB}} - \phi_c)$ in (3) and (4) can be determined, and it can further be applied to solve equations

$$\left\{ \begin{array}{l} (\phi_c - \phi_{\mathrm{LSB}}) = \phi_c - 2\pi f_{\mathrm{LSB}} \dfrac{\mathrm{dis}}{c} \\ (\phi_{\mathrm{HSB}} - \phi_c) = 2\pi f_{\mathrm{HSB}} \dfrac{\mathrm{dis}}{c} - \phi_c \end{array} \right\}. \tag{5}$$

In (5), there are two unknown variables dis and ϕ_c, which can be determined by bringing the results from (3) and (4). Knowing dis and ϕ_c, the secondary nodes compensate the phase offset and synchronize with primary node. However, all the nodes have free running LOs with no reference clock, and the secondary nodes keep sampling without aligning with the time point at which primary node sends out sequential sideband signals, which causes significant phase error in secondary nodes phase compensation process. Therefore, a time offset t_0 is applied to indicate the time difference between the time point primary node sending out the sequential SSB signals and the sampling time point at the secondary nodes. With this t_0, (3) and (4) are rewritten as

$$\mathrm{IF}_{\mathrm{LSB}}(t) = 0.5 \cdot \cos[2\pi(f_{\mathrm{LO}} - f_{\mathrm{LSB}})(t + t_0) + (\phi_c - \phi_{\mathrm{LSB}})] \tag{6}$$

$$\mathrm{IF}_{\mathrm{HSB}}(t) = 0.5 \cdot \cos[2\pi(f_{\mathrm{HSB}} - f_{\mathrm{LO}})(t + t_0) + (\phi_{\mathrm{HSB}} - \phi_c)]. \tag{7}$$

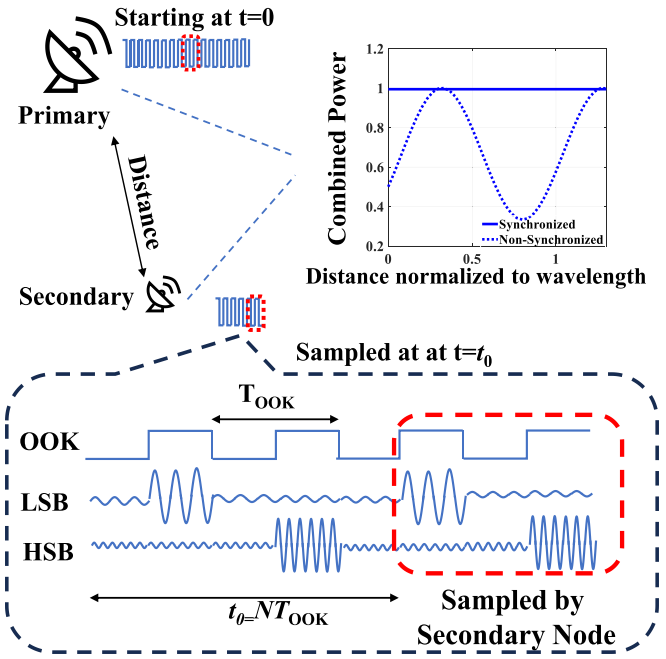

Fig. 2. Comparation between synchronized signal and unsynchronized signal power on the target with a sweep of distance between primary and secondary node.

After sampling and Fourier transformation, the phases in (6) and (7) are noted as φ_{LSB} and φ_{HSB}, and they are derived as

$$\varphi_{\mathrm{LSB}} = 2\pi f_{\mathrm{LSB}} t_0 + \phi_c - \phi_{\mathrm{LSB}} \tag{8}$$

$$\varphi_{\mathrm{HSB}} = 2\pi f_{\mathrm{HSB}} t_0 + \phi_{\mathrm{HSB}} - \phi_c. \tag{9}$$

Due to the randomness of t_0, the secondary nodes are not able to determine the phase offset from (8) and (9). To overcome this problem, on–off keying (OOK) modulation is applied to the sequentially switched SSB signal sent from the primary node. Here, the period length of the OOK signal T_{OOK} is a common multiple periods of LSB signal T_{LSB} and HSB signal T_{HSB}, which follows $T_{\mathrm{OOK}} = nT_{\mathrm{LSB}} = mT_{\mathrm{HSB}}$, $\{m, n \in N | m, n \geq 0\}$. As shown in Fig. 2, $t_0 = NT_{\mathrm{OOK}}$ at secondary nodes, where the time offset t_0 reflects into OOK modulation width T_{OOK}. Here, N is an integer greater than 0. Therefore, it can be simplified as $t_0 = NT_{\mathrm{OOK}} = NnT_{\mathrm{LSB}} = NmT_{\mathrm{HSB}}$. Applying this relation, (8) and (9) can be derived as

$$\varphi_{\mathrm{LSB}} = 2Nn\pi + (\phi_c - \phi_{\mathrm{LSB}}) \tag{10}$$

$$\varphi_{\mathrm{HSB}} = 2Nm\pi + (\phi_{\mathrm{LSB}} - \phi_c). \tag{11}$$

Thus, φ_{LSB} and φ_{HSB} are independent of t_0, and dis and ϕ_c can be solved following (5), so that the secondary nodes synchronize the phases with the primary node. The comparison of the combined signal received by the target with and without synchronization in the distributed array is illustrated in Fig. 2. Without synchronization, from (1) and (2), the combined power varies periodically across distance, which is normalized to the wavelength of the transmitted signals. Conversely, with the proposed phase synchronization methodology, the combined power reaches its maximum and is constant across the distance.

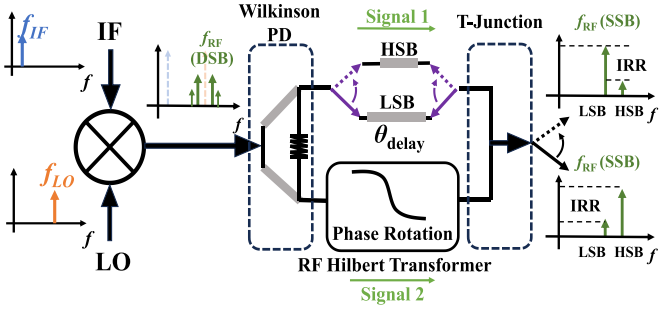

Fig. 3. Proposed RF Hilbert transformer SSB mixer topology.

B. Design of Switchable RF/Analog Processing SSB Mixer

From the above analysis of the proposed phase synchronization procedure in an open-loop distributed array, the critical step is generating a switchable sideband signal for phase synchronization with high spectrum efficiency. Unlike conventional SSB mixers, in this extended paper, a novel switchable sideband SSB mixer is derived from an RF Hilbert transformer and switchable delay lines, and the circuit topology is shown in Fig. 3. A single balanced mixer converts IF to RF by mixing with LO, and then, the output signal is divided into two paths through a Wilkinson power divider. One branch signal is processed by an RF Hilbert transformer, which rotates signal phase by 180° directly at RF center frequency without changing its magnitude, so that the LSB signal and HSB signal are directly processed to 180° offset from each other. The other branch wave passes along a switchable transmission line delay, which can be controlled to reject either the LSB signal or the HSB signal. After combining the two branch signals via a zero-degree power combiner, one sideband signal will be canceled out due to 180° phase offset between two sideband signals from the RF Hilbert transformation and the delay line. For example, to reject the HSB signal, the delay line is switched to a small electrical length transmission line, and LO + IF upper sideband undergoes a 180° phase rotation via RF Hilbert transformer, so that the combined signal only contains the LSB signal.

The key building block in the proposed switchable SSB mixer is the RF Hilbert transformer, which is composed of a 180° rat-race coupler and a feedback delay line. The ideal transfer function of the Hilbert transformer is

$$\begin{aligned} y(t) &= \mathrm{HT}[x(t)] \\ &= \frac{1}{\pi} p.v. \int_{-\infty}^{+\infty} \frac{x(\tau)}{t-\tau} d\tau \end{aligned} \tag{12}$$

where the Cauchy principal value is denoted as $p.v$. Its Fourier transformation can be expressed as

$$Y(\omega) = \mathrm{HT}(\omega) \cdot X(\omega). \tag{13}$$

The phase response of the ideal transfer function $\mathrm{HT}(\omega)$ shows a sharp 180° rotation at the center frequency, while the magnitude remains constant in the frequency band, as shown in Fig. 4, which is foundational to enable sideband cancellation in the proposed switchable SSB mixer. To realize the Hilbert transformation transfer function directly at high

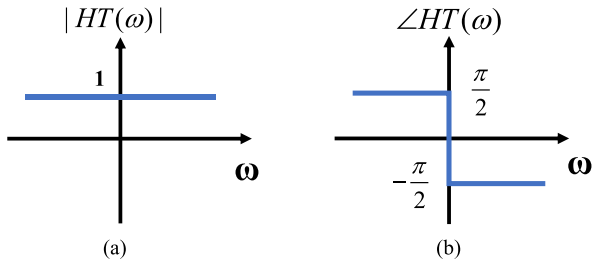

Fig. 4. Transfer function of ideal Hilbert transformation. (a) Magnitude response. (b) Phase response.

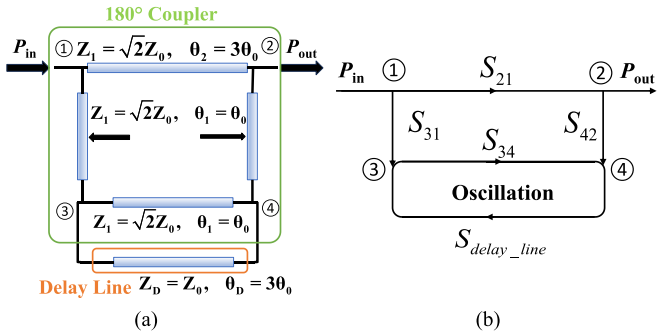

Fig. 5. (a) Transmission line RF Hilbert transformer circuit. (b) Signal flowchart analysis of RF Hilbert transformer.

frequencies, a transmission line topology is proposed and shown in Fig. 5(a), where $Z_1 = \sqrt{2}Z_0$, $Z_D = Z_0$, $\theta_1 = \theta_0$, and $\theta_2 = 3\theta_0$. Here, $Z_0 = 50\ \Omega$ and $\theta_0 = 90°$. The feedback transmission line between ports ③ and ④ follows the rule that $\theta_D + \theta_1 = 360°$ forming a resonator. To analyze the proposed circuit, the signal flowchart method shown in Fig. 5(b) is applied to determine its transfer function, which is derived as

$$\mathrm{HT}(f) = S_{21} + \frac{S_{31}S_{\mathrm{delay\_line}}S_{42}}{1 - S_{34}S_{\mathrm{delay\_line}}} \tag{14}$$

where S_{21} is the transmission from input port ① to output port ②. S_{31} and S_{42} are the couplings from ③ to ① and ④ to ②, respectively. S_{34} is the transmission from ③ to ④. $S_{\mathrm{delay\_line}}$ is the feedback delay line connecting port ③ and ④ to maintain the resonance. The magnitude and phase responses of the RF Hilbert transformer for both theoretical (solid line) and EM simulation (dashed line) are shown in Fig. 6, where a 180° phase rotation is clearly observed at the center LO frequency without significant magnitude changes. Here, the small magnitude deviation at center frequency is caused from dielectric loss of microstrip line-based resonator in RF Hilbert transformer. Also, the bandwidth limitation of coupler in RF Hilbert transformer causes magnitude roll off at two edge frequencies.

With the RF Hilbert transformer design, the single balanced mixer in the proposed switchable sideband SSB mixer shown in Fig. 3 is designed using two Schottky diodes connected in an antipolar configuration and one rat-race coupler. The LO signal is applied to the delta port of the rat-race coupler, and the IF signal is fed to the anti-polar diode pair via a low-pass filter. Due to the nonlinearity of diode, the two signal LO and IF are mixed and upconverted to a double sideband (DSB)

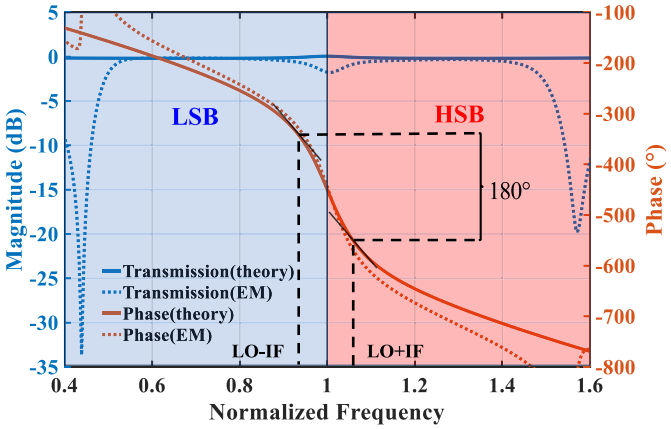

Fig. 6. Magnitude and phase responses of proposed RF Hilbert transformer.

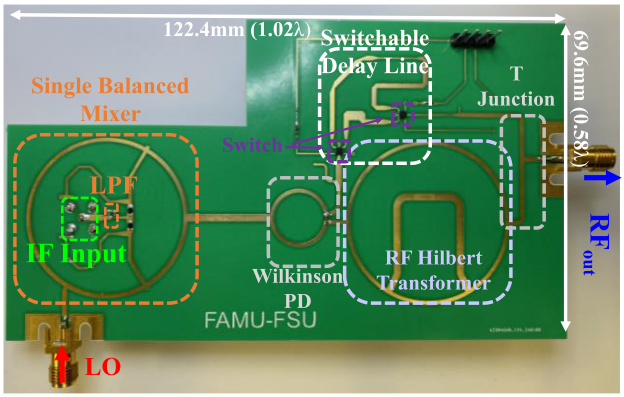

Fig. 7. Prototype of proposed RF/analog processing switchable SSB mixer.

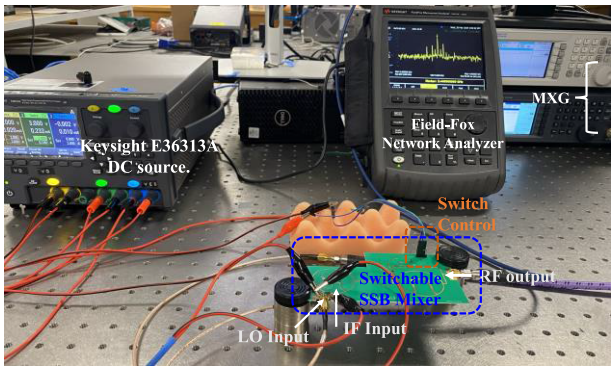

Fig. 8. Experimental setup for validating the proposed RF/analog processing switchable SSB mixer.

output, which is derived as [33]

$$v_{\mathrm{DSB}}(t) = v_{\mathrm{LO+IF}}(t) + v_{\mathrm{LO-IF}}(t) \tag{15}$$

$$v_{\mathrm{LO-IF}}(t) = \frac{V_{\mathrm{RF}}}{2}\cos[(\omega_{\mathrm{LO}} - \omega_{\mathrm{IF}})t] \tag{16}$$

$$v_{\mathrm{LO+IF}}(t) = \frac{V_{\mathrm{RF}}}{2}\cos[(\omega_{\mathrm{LO}} + \omega_{\mathrm{IF}})t]. \tag{17}$$

The output from the single balanced mixer, including LO + IF and LO-IF frequency components, is equally divided into two paths via a Wilkinson power divider. One path is transferred by RF Hilbert transformer, and the other branch is path through the switchable transmission line delay providing

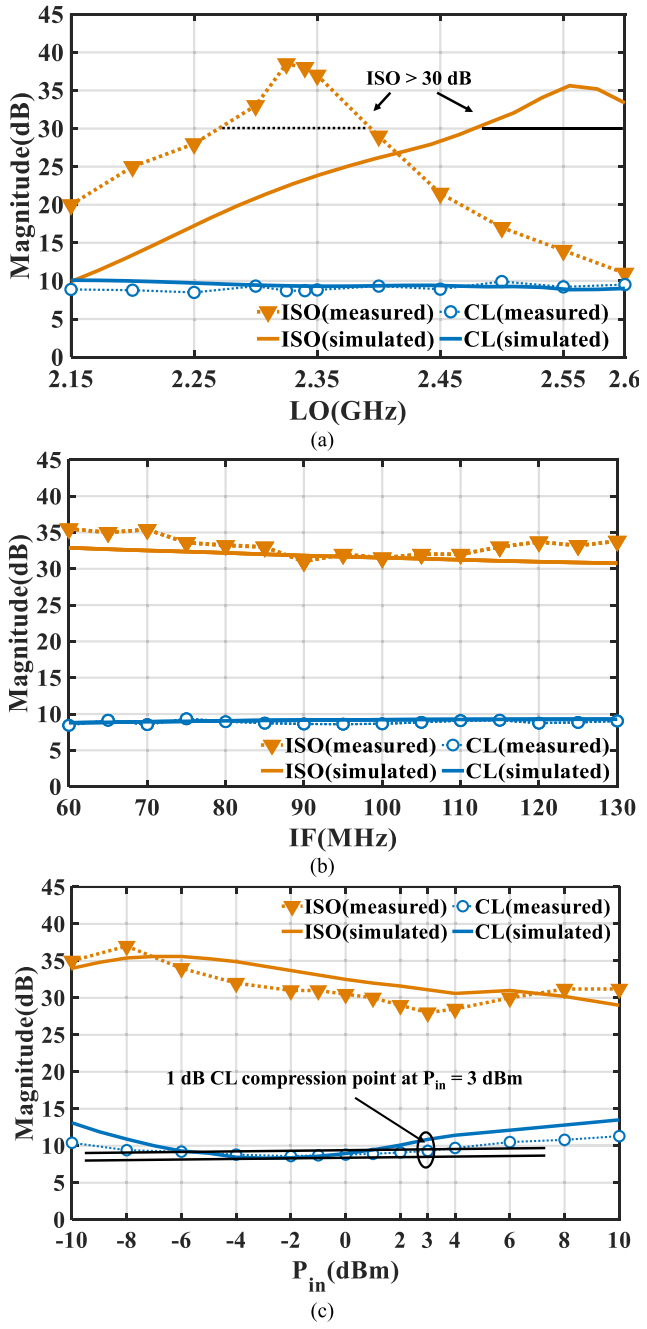

Fig. 9. Performance of ISO and CL of applied single balanced mixer with (a) LO frequency sweep, (b) IF frequency sweep, and (c) input power (P_{in}) sweep, where the same P_{in} is applied to both the LO and IF. In these plots, the center LO frequency for measurement and simulation is set to be 2.34 and 2.5 GHz separately. Default P_{in} and IF frequency is set to be 0 dBm and 100 MHz.

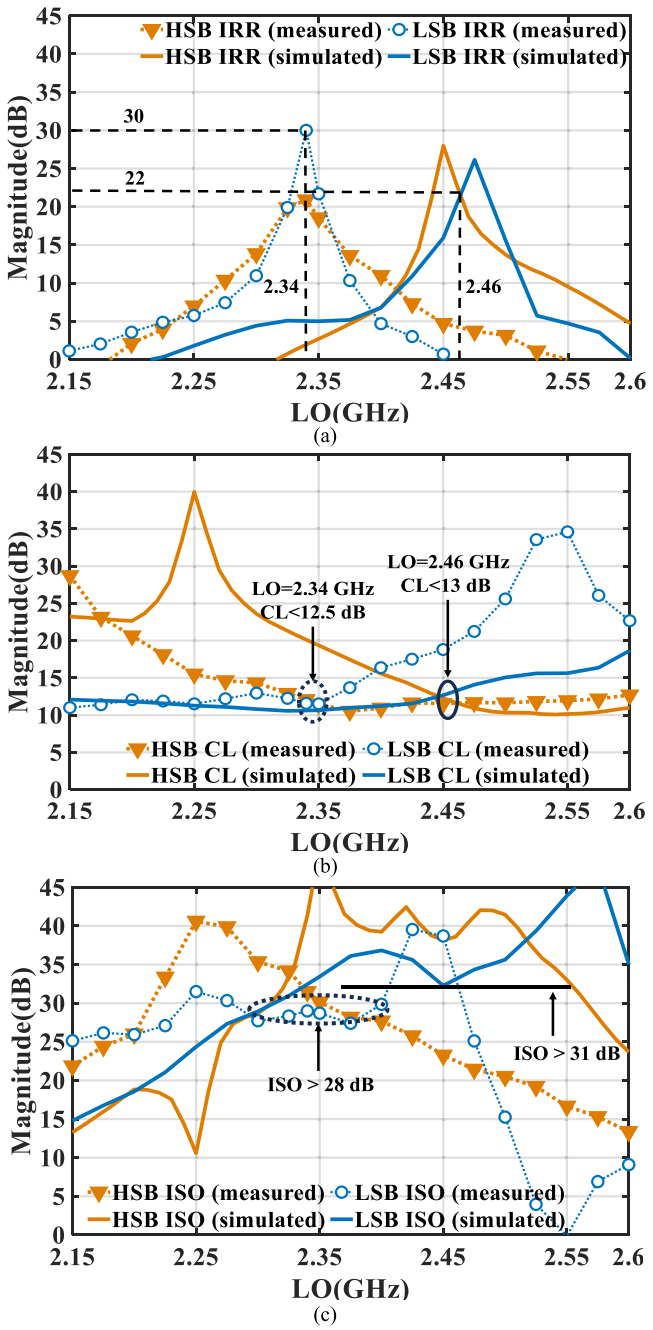

Fig. 10. Simulated and measured performance of both HSB and LSB of the proposed switchable SSB mixer with a sweep of LO frequency versus (a) image rejection ratio, (b) conversion loss, and (c) ISO. IF for both measurement and simulation is 100 MHz. P_{in} is 0 dBm.

phase offset with signal transformed by RF Hilbert transformer. The signal passing through switchable transmission line delay can be derived as

$$v_{\text{Signal1}}(t) = \frac{1}{\sqrt{2}} V_{\text{DSB}}[\cos(\omega_{\text{LO+IF}} t + \theta_{\text{delay}})] + \frac{1}{\sqrt{2}} V_{\text{DSB}}[\cos(\omega_{\text{LO-IF}} t + \theta_{\text{delay}})] \quad (18)$$

where θ_{delay} notes the electrical length of switchable transmission line. The signal passing through RF Hilbert transformer can be derived as

$$v_{\text{Signal2}}(t) = \frac{1}{\sqrt{2}} V_{\text{DSB}}[\cos(\omega_{\text{LO+IF}} t + \theta_{\text{HT}})] + \frac{1}{\sqrt{2}} V_{\text{DSB}}[\cos(\omega_{\text{LO-IF}} t)] \quad (19)$$

where θ_{HT} notes the phase rotation from the RF Hilbert transformer in (14). The delayed signal in (18) and RF Hilbert transformed signals in (19) are combined through T-combiner,

and the output is derived as

$$\begin{aligned} v_{\mathrm{SSB}}(t) &= v_{\mathrm{Signal1}}(t) + v_{\mathrm{Signal2}}(t) \\ &= \frac{1}{\sqrt{2}} V_{\mathrm{DSB}}[\cos(\omega_{\mathrm{LO+IF}}t + \theta_{\mathrm{HT}}) + \cos(\omega_{\mathrm{LO+IF}}t + \theta_{\mathrm{delay}})] \\ &\quad + \frac{1}{\sqrt{2}} V_{\mathrm{DSB}}[\cos(\omega_{\mathrm{LO-IF}}t) + \cos(\omega_{\mathrm{LO-IF}}t + \theta_{\mathrm{delay}})]. \quad (20) \end{aligned}$$

From (18), the SSB output $v_{\mathrm{SSB}}(t)$ is composed of both HSB and LSB signals from the two branches. Applying (15)–(17) into (20) and setting $\theta_{\mathrm{HT}} = \pi$ for HSB signal, the sideband selection will be determined by electrical length of the delay line θ_{delay}. For HSB cancellation, θ_{delay} is set to be 0°, and θ_{delay} is 180° for LSB cancellation.

III. Implementation of the Proposed Switchable RF/Analog Processing SSB Mixer

To prove the design concept, the proposed switchable SSB mixer is designed and fabricated using RO4350B PCB with a substrate thickness of 0.76 mm, $\varepsilon_r = 3.48$, and $\tan\delta = 0.0037$. The prototype is shown in Fig. 7, and the size is 122.4 × 69.6 mm ($1.02\lambda \times 0.58\lambda$, where λ denotes the wavelength). In this design, the LO frequency is 2.46 GHz, and the IF frequency is 100 MHz. The prototype switchable sideband SSB mixer comprises a single-balanced mixer, Wilkinson power divider, RF Hilbert transformer, RF switches (PE42424), transmission line delay lines, and 0° combiner. Here, the electrical length of transmission line delay lines in switchable delay line is either 0 or π. Also, a T-junction combiner is designed for realizing a 0° power combiner to combine signals passing through switchable delay lines and RF Hilbert transformer without isolation (ISO). The circuit simulation, layout design, and EM simulation are carried out using Keysight ADS, and the experimental setup for the proposed SSB mixer is shown in Fig. 8, where IF and LO sources are generated from two signal generators (MXG). To determine the center frequency of the prototype, LO frequency is swept using a Keysight EXG N5172B to find the minimum conversion loss (CL) with low IRR, and IF frequency is fixed from Agilent N5181A. The two RF switches are controlled by a Keysight E36313A dc power supply to determine difference sideband cancellation. The performance of the proposed switchable sideband SSB mixer in LSB or HSB cancellation is characterized separately by configuring two different sets of dc voltage for RF switches. The spectrum of the output signal from switchable SSB mixer is measured using a Keysight FieldFox microwave vector network analyzer.

A two-step experiment is carried out to fully characterize the performance of the proposed switchable sideband SSB mixer. First, the single-balanced mixer shown in Fig. 7 is measured, and the simulations and measurement results are correlated and shown in Fig. 9. Specifically, the ISOs between LO input and RF output and the CLs from IF input to RF output with f_{LO} sweep from 2.15 to 2.6 GHz are shown in Fig. 9(a). By applying identical input power (0 dBm) for both LO and IF, the ISO is better than 30 dB within a 100-MHz bandwidth for both simulation and measurement, while the CLs are smaller

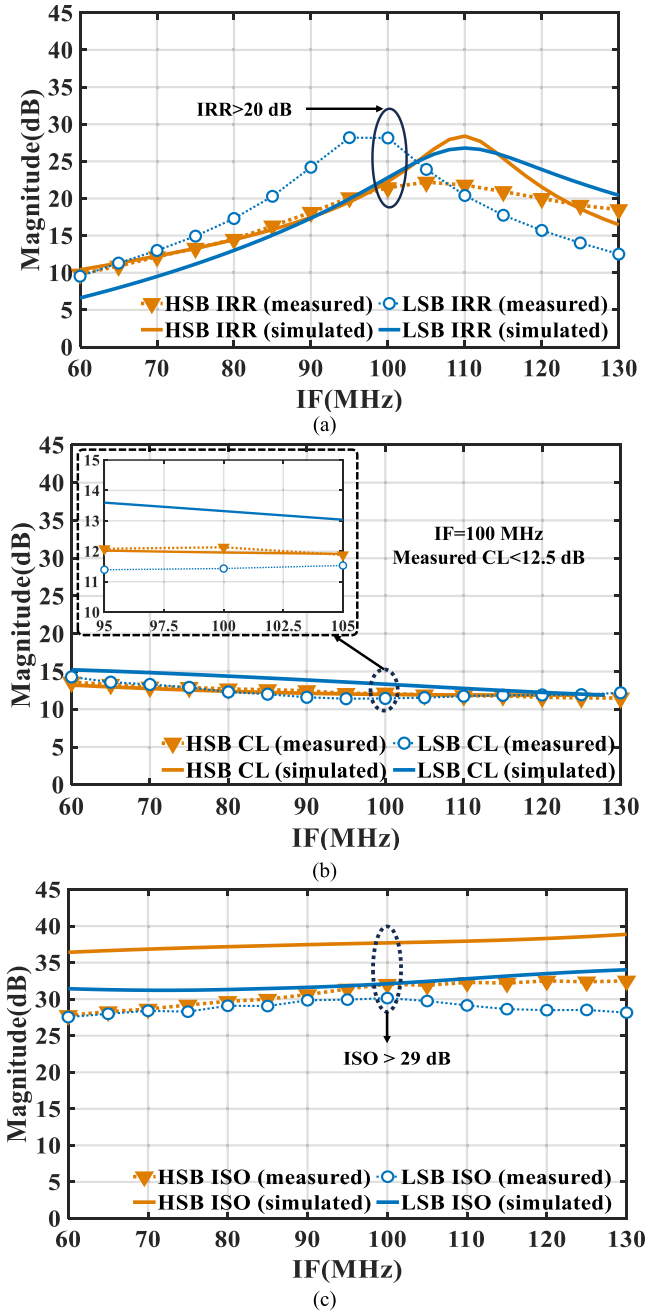

Fig. 11. Simulated and measured performance of both HSB and LSB of the proposed switchable SSB mixer with IF frequency sweep versus (a) image rejection ratio, (b) conversion loss, and (c) ISO. LO center frequency is 2.5 and 2.34 GHz at simulation and measurement, respectively. P_{in} is 0 dBm.

than 10 dB across the LO sweep. On the other hand, ISO and CL are measured by sweeping f_{IF} from 60 to 130 MHz, as shown in Fig. 9(b). The ISOs are larger than 31 dB and CLs are smaller than 10.5 dB in both simulation and measurement results. In addition, the input power level for both IF and LO signals is swept (−10 to 10 dBm) to characterize the linearity of the single-balanced mixer. As shown in Fig. 9(c), with $f_{\mathrm{LO}} = 2.5$ GHz and $f_{\mathrm{IF}} = 100$ MHz, the ISOs are greater than 31 dB. For the P_{in} sweep, CL is varying in a range of 9–13 dB, and the minimum CL value is both simulated and measured at $P_{\mathrm{in}} = -2$ dBm. The linearity of the mixer

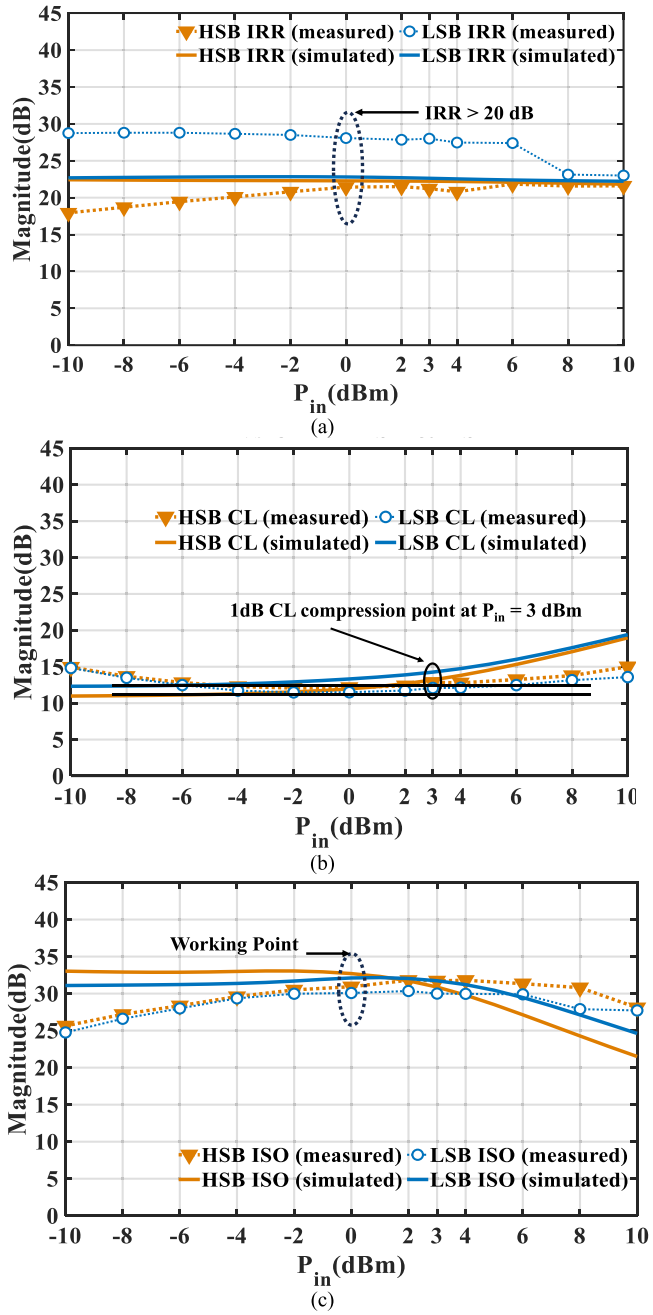

Fig. 12. Simulation and measurement of HSB and LSB for the proposed SSB mixer with input power (P_{in}) sweep, where the same P_{in} is applied to both the LO and IF versus (a) image rejection ratio, (b) conversion loss, and (c) ISO. IF is 100 MHz, and LO center frequency is 2.5and 2.34 GHz at simulation and measurement, respectively.

is quantified from the CL variation since CL $= P_{\text{in}} - P_{\text{out}}$, and it is plotted with the P_{in} sweep, as shown in Fig. 9(c). The simulated and measured 1-dB compression point of the proposed single balanced mixer is at $P_{\text{in}} = 3$ dBm.

In the second experiment, the proposed RF/analog processing switchable SSB mixer is measured and correlated with simulation, and the results are shown in Fig. 10, where $f_{\text{IF}} = 100$ MHz, $f_{\text{LO}} = 2.15$–2.6 GHz, and $P_{\text{in}} = 0$ dBm for both IF and LO signal. The simulated and measured image rejection ratios are shown in Fig. 10(a), where the simulated IRR is greater than 21 dB at $f_{\text{LO}} = 2.46$ GHz for both LSB and HSB cancellation modes. The measured IRR is about 30 dB for LSB mode and 20 dB for HSB mode at $f_{\text{LO}} = 2.34$ GHz. The simulations and measurements of CLs are shown in Fig. 10(b). It can be observed that the simulated CLs for two modes are better than 13 dB at $f_{\text{LO}} = 2.46$ GHz, while the measured CLs are smaller than 12.5 dB at $f_{\text{LO}} = 2.34$ GHz. Compared to a single balanced mixer, the proposed switchable sideband mixer exhibits a 2.5-dB offset in the CL, which arises from mismatches between single balanced mixer and sideband selection circuit, including power divider, RF switches, RF Hilbert transformer, and power combiner, particularly in power sweep measurements. Fig. 10(c) shows the simulation and measurement results of ISO, which are better than 28 dB in simulation and greater than 31 dB in the experiment at the corresponding f_{LO}, respectively.

The slight frequency offset between simulation and measurement is mainly caused from manufacturing tolerance and accuracy of nonlinear device model. Similarly, the proposed switchable SSB mixer is also characterized by sweeping IF frequency from 60 to 130 MHz, and the results are shown in Fig. 11. From the simulation and measurement results, it is found that the mixer shows optimum performance at an IF frequency of 100 MHz in both simulations and measurements. Specifically, the IRR is greater than 20 dB for both LSB and HSB cancellation modes shown in Fig. 11(a). In Fig. 11(b) and (c), the CLs and ISOs range between 12.5 and 29 dB, respectively. The linearity of the proposed switchable SSB mixer is also characterized by sweeping of P_{in} from -10 to 10 dBm, where the same P_{in} is applied to both the LO and IF signal. In Fig. 12(a), the simulated IRRs for both LSB and HSB cancellation modes are around 22.5 dB, while the measured IRRs are better than 27 dB in LSB mode and better than 17 dB in HSB cancellation mode. Fig. 12(b) shows the CL responses of the proposed switchable sideband SSB mixer across input power sweep, and its 1-dB compression points are at $P_{\text{in}} = 3$ dBm for both simulation and measurement. The ISO simulation and measurement results of the proposed switchable sideband SSB mixer are shown in Fig. 12(c), where the simulation is better than 30 dB while measurement is greater than 25 dB.

From the analysis of simulation and measurement results, it finds a frequency offset and a small performance discrepancy, which is caused by several factors. One reason arises from the sensitivity of RF Hilbert transformer, where a slight electrical length error can change the frequency response, thereby degrading the overall performance of sideband cancellation. Another reason is from the modeling of active elements as diode and RF switch. In current design, the available S-parameters are applied for modeling of RF switch, which leads to significant variance in power sweep simulations and measurements of the proposed switchable sideband SSB mixer.

In summary, the proposed switchable sideband RF/analog processing SSB mixer has demonstrated to achieve robust performance in all aspects for spectrum-efficient distributed array phase synchronization. To differentiate from other SSB mixer topologies, including active and photonic-based mixers, the comparison is shown in Table I. Passive SSB mixers [19],

TABLE I
COMPARISON OF SSB MIXER PERFORMANCE

Ref.	f_0 (GHz)	SSB CL (dB)	ISO (dB)	IRR (dB)	Switchable	IP1dB(dBm)	Active/Passive	P_{diss}(mW)	Technology	Size(mm^2)
[19]	16	10	/	30	No	/	Passive	0	MMIC	216
[22]	2.44	11	/	15-18	No	/	Passive	0	65nm CMOS	0.44
[34]	5.65	15	31	30	No	3	Passive	0	PCB	1155
[35]	2.5	14	N.A.	>20	No	-8	Passive	0	PCB	1800
[36]	75-90	11	>30	>20	No	7	Passive	0	MMIC	3
[37]	3.09-3.51	/	/	>40	No	/	Active	49.12-52.62	0.18μm CMOS	/
[38]	3.43-10.3	/	/	19-40	No	/	Active	/	0.13μm CMOS	~0.03
[40]	11	6	/	>40	No	/	Passive	/	Photonic Based	/
T. W.	2.34	11.5	30	21.5	Yes	3	Passive	0	PCB	8519

[24], [25], [26] show a close conversion loss around 10 dB, while having different IRR varying from 19 to over 40 dB depending on the architectures and fabrication. On the other hand, active device mixers [27], [28] employ transistor pairs to show smaller size. In [29], a classical SSB topology achieves an IRR of 15–18 dB but with limited LO ISO due to its architecture. The photonic-based SSB mixer in [30] enables a high IRR over 40 dB but has bulky size, which is challenging for compact integration. Compared to other works, our proposed SSB mixer features a controllable sideband switching characteristic with comparable performance, including IRR, CL, ISO, and IP1 dB, which has great potential to be applied in developing novel wireless systems.

IV. CONCLUSION

A novel RF/analog processing switchable SSB mixer is proposed in this article to synchronize the phase in an open-loop distributed array. The design theory is derived for phase synchronization and the switchable SSB mixer, and the prototype of the proposed SSB mixer is designed and validated in experiments to prove the design concept. A slight frequency offset is observed between simulation and measurement, which is mainly due to the model of nonlinear devices and fabrication tolerance. The performance of the proposed SSB mixer is limited by the microstrip line rat-race coupler. In the next step, authors will further investigate a compact size wideband proposed SSB mixer. This is the first time a novel circuit topology is proposed for SSB mixer design to feature a sideband switching characteristic. In the next step, a novel transceiver system integrating the proposed switchable sideband SSB mixer will be developed to construct a distributed array system and experimentally demonstrate its phase synchronization.

REFERENCES

[1] H. Ren, B. Arigong, M. Zhou, J. Ding, and H. Zhang, "A novel design of 4 × 4 Butler matrix with relatively flexible phase differences," *IEEE Antennas Wireless Propag. Lett.*, vol. 15, pp. 1277–1280, 2016.

[2] H. Ren, H. Zhang, Y. Jin, Y. Gu, and B. Arigong, "A novel 2-D 3 × 3 nolen matrix for 2-D beamforming applications," *IEEE Trans. Microw. Theory Techn.*, vol. 67, no. 11, pp. 4622–4631, Nov. 2019.

[3] H. Zhang, H. Ren, P. Liu, H. Yan, and B. Arigong, "Tunable 3 × 3 nolen matrix network for power-saving phased array," *IEEE Microw. Wireless Technol. Lett.*, vol. 34, no. 8, pp. 995–998, Aug. 2024.

[4] B.-H. Ku et al., "A 77–81-GHz 16-element phased-array receiver with ±50° beam scanning for advanced automotive radars," *IEEE Trans. Microw. Theory Techn.*, vol. 62, no. 11, pp. 2823–2832, Nov. 2014.

[5] Y. Yin, B. Ustundag, K. Kibaroglu, M. Sayginer, and G. M. Rebeiz, "Wideband 23.5–29.5-GHz phased arrays for multistandard 5G applications and carrier aggregation," *IEEE Trans. Microw. Theory Techn.*, vol. 69, no. 1, pp. 235–247, Jan. 2021.

[6] P. K. Bailleul, "A new era in elemental digital beamforming for spaceborne communications phased arrays," *Proc. IEEE*, vol. 104, no. 3, pp. 623–632, Mar. 2016.

[7] T. Choi, P. Luo, A. Ramesh, and A. F. Molisch, "Co-located vs distributed vs semi-distributed MIMO: Measurement-based evaluation," in *Proc. 54th Asilomar Conf. Signals, Syst., Comput.*, Nov. 2020, pp. 836–841.

[8] O. Abari, H. Rahul, D. Katabi, and M. Pant, "AirShare: Distributed coherent transmission made seamless," in *Proc. IEEE Conf. Comput. Commun. (INFOCOM)*, Apr. 2015, pp. 1742–1750.

[9] R. Mudumbai, D. R. B. Iii, U. Madhow, and H. V. Poor, "Distributed transmit beamforming: Challenges and recent progress," *IEEE Commun. Mag.*, vol. 47, no. 2, pp. 102–110, Feb. 2009.

[10] M. Seo, M. Rodwell, and U. Madhow, "A feedback-based distributed phased array technique and its application to 60-GHz wireless sensor network," in *IEEE MTT-S Int. Microw. Symp. Dig.*, Jun. 2008, pp. 683–686.

[11] P. Bidigare et al., "Implementation and demonstration of receiver-coordinated distributed transmit beamforming across an ad-hoc radio network," in *Proc. Conf. Rec. 46th Asilomar Conf. Signals, Syst. Comput. (ASILOMAR)*, Nov. 2012, pp. 222–226.

[12] S. Shi, S. Zhu, X. Gu, and R. Hu, "Extendable carrier synchronization for distributed beamforming in wireless sensor networks," in *Proc. Int. Wireless Commun. Mobile Comput. Conf. (IWCMC)*, Paphos, Cyprus, Sep. 2016, pp. 298–303.

[13] R. Mudumbai, G. Barriac, and U. Madhow, "On the feasibility of distributed beamforming in wireless networks," *IEEE Trans. Wireless Commun.*, vol. 6, no. 5, pp. 1754–1763, May 2007.

[14] B. Luo, P. L. Yeoh, R. Schober, and B. S. Krongold, "Distributed multiantenna frequency-selective energy beamforming with joint total and individual power constraints," *IEEE Trans. Green Commun. Netw.*, vol. 6, no. 4, pp. 2100–2114, Dec. 2022.

[15] M. Rashid and J. A. Nanzer, "Frequency and phase synchronization in distributed antenna arrays based on consensus averaging and Kalman filtering," *IEEE Trans. Wireless Commun.*, vol. 22, no. 4, pp. 2789–2803, Apr. 2023.

[16] S. R. Mghabghab and J. A. Nanzer, "Open-loop distributed beamforming using wireless frequency synchronization," *IEEE Trans. Microw. Theory Techn.*, vol. 69, no. 1, pp. 896–905, Jan. 2021.

[17] S. M. Ellison, S. R. Mghabghab, and J. A. Nanzer, "Multi-node open-loop distributed beamforming based on scalable, high-accuracy ranging," *IEEE Sensors J.*, vol. 22, no. 2, pp. 1629–1637, Jan. 2022.

[18] S. R. Mghabghab, S. M. Ellison, and J. A. Nanzer, "Open-loop distributed beamforming using wireless phase and frequency synchronization," *IEEE Microw. Wireless Compon. Lett.*, vol. 32, no. 3, pp. 234–237, Mar. 2022.

[19] C.-Y. Chi and G. M. Rebeiz, "Design of lange-couplers and single-sideband mixers using micromachining techniques," *IEEE Trans. Microw. Theory Techn.*, vol. 45, no. 2, pp. 291–294, Feb. 1997.

[20] K. Hettak, G. A. Morin, and M. G. Stubbs, "A novel miniature multilayer MMIC CPW single side band CPW mixer for up conversion at 44.5 GHz," *IEEE Microw. Wireless Compon. Lett.*, vol. 15, no. 9, pp. 606–608, Sep. 2005.

[21] H.-J. Wei, C. Meng, T.-W. Wang, T.-L. Lo, and C.-L. Wang, "60-GHz dual-conversion down-/up-converters using Schottky diode in 0.18 μm foundry CMOS technology," *IEEE Trans. Microw. Theory Techn.*, vol. 60, no. 6, pp. 1684–1698, Jun. 2012.

[22] M. Meng et al., "12.2 improving the range of WiFi backscatter via a passive retro-reflective single-side-band-modulating MIMO array and non-absorbing termination," in *IEEE Int. Solid-State Circuits Conf. (ISSCC) Dig. Tech. Papers*, vol. 64, Feb. 2021, pp. 202–204.

[23] Y. Liu, B. Zhang, Z. Niu, Y. Feng, and Y. Fan, "A novel 180–210 GHz single sideband mixer using filtering waveguide-microstrip transition structure," *IEEE Microw. Wireless Technol. Lett.*, vol. 33, no. 6, pp. 727–730, Jun. 2023.

[24] W. Liu et al., "A fully reconfigurable photonic integrated signal processor," *Nature Photon.*, vol. 10, no. 3, pp. 190–195, Mar. 2016.

[25] H. V. Nguyen and C. Caloz, "First- and second-order differentiators based on coupled-line directional couplers," *IEEE Microw. Wireless Compon. Lett.*, vol. 18, no. 12, pp. 791–793, Dec. 2008.

[26] J. D. Schwartz, J. Azana, and D. V. Plant, "An electronic temporal imaging system for compression and reversal of arbitrary UWB waveforms," in *Proc. IEEE Radio Wireless Symp.*, Jan. 2008, pp. 487–490.

[27] M. A. G. Laso et al., "Real-time spectrum analysis in microstrip technology," *IEEE Trans. Microw. Theory Techn.*, vol. 51, no. 3, pp. 705–717, Mar. 2003.

[28] H. Zhang and B. Arigong, "A novel frequency reconfigurable real-time RF edge detector," in *IEEE MTT-S Int. Microw. Symp. Dig.*, Jun. 2023, pp. 1148–1151.

[29] A. El Sayed et al., "A Hilbert transform equalizer enabling 80 MHz RF self-interference cancellation for full-duplex receivers," *IEEE Trans. Circuits Syst. I, Reg. Papers*, vol. 66, no. 3, pp. 1153–1165, Mar. 2019.

[30] R. Islam, M. H. Maktoomi, H. Ren, and B. Arigong, "Spectrum aggregation dual-band real-time RF/microwave analog signal processing from microstrip line high-frequency Hilbert transformer," *IEEE Trans. Microw. Theory Techn.*, vol. 69, no. 11, pp. 4647–4657, Nov. 2021.

[31] H. P. Bazargani, M. R. Fernández-Ruiz, and J. Azana, "Tunable optical filter using photonic Hilbert transformation," *Adv. Photon.*, vol. 2013, pp. 1–3, Jul. 2013.

[32] H. Yan et al., "A novel RF Hilbert transformer single sideband mixer," in *IEEE MTT-S Int. Microw. Symp. Dig.*, Jun. 2024, pp. 624–627.

[33] B. Razavi, *Fundamentals of Microelectronics*, 2nd ed., Hoboken, NJ, USA: Wiley, 2013.

[34] H.-Y. La and Y.-C. Chiang, "A novel structure of single-side-band mixer with adopting dual-band quadrature coupler," in *Proc. Asia–Pacific Microw. Conf.*, Dec. 2009, pp. 701–704.

[35] Y.-C. Chiang and M.-C. Ma, "Wide-band single-side band subharmonic mixer constructed with re-entrant couplers and lumped-element coupler," *IEEE Microw. Wireless Compon. Lett.*, vol. 18, no. 12, pp. 806–808, Dec. 2008.

[36] Y. Ye, J. Zhang, R. Tong, and X. Sun, "A linear resistive single sideband (SSB) up-converter for E-band wireless communication," in *Proc. IEEE Int. Wireless Symp. (IWS)*, Mar. 2014, pp. 1–4.

[37] D. Huang, W. Li, J. Zhou, N. Li, and J. Chen, "A frequency synthesizer with optimally coupled QVCO and harmonic-rejection SSBmixer for multi-standard wireless receiver," *IEEE J. Solid-State Circuits*, vol. 46, no. 6, pp. 1307–1320, Jun. 2011.

[38] S. Rong, J. Yin, and H. C. Luong, "A 0.05- to 10-GHz, 19- to 22-GHz, and 38- to 44-GHz frequency synthesizer for software-defined radios in 0.13- μm CMOS process," *IEEE Trans. Circuits Syst. II, Exp. Briefs*, vol. 63, no. 1, pp. 109–113, Jan. 2016.

[39] M. Meng et al., "Improving the range of WiFi backscatter via a passive retro-reflective single-side-band-modulating MIMO array and non-absorbing termination," in *IEEE Int. Solid-State Circuits Conf. (ISSCC) Dig. Tech. Papers*, Feb. 2021, pp. 1–4.

[40] Z. Tang and S. Pan, "A filter-free photonic microwave single sideband mixer," *IEEE Microw. Wireless Compon. Lett.*, vol. 26, no. 1, pp. 67–69, Jan. 2016.